

Induced stress arising in crystalline silicon under exposure to ultra-short laser pulses of different duration in air and water

© N.A. Smirnov, S.I. Kudryashov, N.N. Melnik, P.M. Papilova, I.A. Sherstnev, A.A. Ionin, J. Chen

Lebedev Physical Institute, Russian Academy of Sciences, Moscow, Russia

e-mail: cna1992@mail.ru

Received on June 08, 2021

Revised on June 23, 2021

Accepted on July 25, 2021

The silicon surface was modified in a single-pulse mode with femto-picosecond laser pulses (0.3 and 10 ps) in the near-IR range (1030 nm) during ablation in air and water. The resulting structures were studied using Raman microscopy. In the course of the study, it was found that nanocrystallites with a size of 7–8 nm appear at the crater boundary. Local mechanical stresses were found in the center of the crater, the sign of which depends on the applied energy density. The highest local compressive stresses arise in water in the subfilamentation mode at maximum energy densities.

Keywords: silicon, Raman spectroscopy, ultrashort pulses, single-pulse ablation in air and liquid, local stresses.

DOI: 10.21883/EOS.2022.13.53988.2399-21

Introduction

Laser ablation is one of the main methods in precision machining in many technological operations, in particular in microelectronics, where silicon is currently the basic element. It is very important, that chemical and phase composition did not change for the laser-treated, as well as nearby areas, and that there are no stresses in the material. For these purposes, ultrashort laser pulses (ULPs, duration less than 10^{-10} s) are the most appropriate, which have the smallest area of thermal action on the material and are increasingly used for laser precision micromachining [1–4].

Local stresses arising after laser machining critically affect the structural reliability of semiconductor devices [5–7]. Therefore, it is important to characterize the residual stress and optimally choose the parameters of laser radiation, at which the stresses arising in silicon are minimal.

Raman spectroscopy (RS) allows to identify a material and provides information about the phonon frequency, electron-phonon interaction, impurities, crystal structure, crystal orientation and mechanical deformation in the material [5–10]. The locality of this method, when focusing with lenses with a large numerical aperture is less than $1\ \mu\text{m}$, which allows us to study the structures obtained by laser in the cross section. Silicon has been well studied in terms of Raman spectroscopy. It is well known, that the peak of the fundamental vibration of crystalline silicon is located at a frequency of $521\ \text{cm}^{-1}$. When silicon is amorphized, the RS is a broad structureless band with a maximum $\sim 480\ \text{cm}^{-1}$ [6]. Any changes and deformations caused by pressure in the material will lead to a shift in the natural vibration frequency in the solid body and will be determined for silicon by the formula [8,9]

$$\sigma\ (\text{MPa}) = -435(\omega - \omega_0)\ (\text{cm}^{-1}), \quad (1)$$

where ω — position of the silicon peak in the unstressed state, ω_0 — position of the silicon peak in the stressed state. In case of lattice disorder the half-widths of the RS bands increase [11,12]. When the size of the crystals decreases to $\sim 2\text{--}10\ \text{nm}$, the selection rules for the wave vector are violated, and the maximum of the RS band shifts towards low frequencies, and the band itself becomes asymmetric: a low-frequency wing of the fundamental vibration appears [13,14]. Based on the shape and position of the RS line in $520\ \text{cm}^{-1}$ region, which is responsible for Si-Si vibrations, from such a spectrum one can estimate the size of nanocrystals.

There is a large number of studies, in which the analysis of laser-induced structures on the silicon surface was carried out, including those under single-pulse laser action [15,16]. At the same time, these studies include no detailed analysis of the obtained structures in the framework of Raman spectroscopy depending on the energy density in the pulse.

In the present study we studied craters obtained by irradiating a silicon wafer with ultrashort laser pulses of variable duration (0.3–10 ps) in air and water media. The craters were characterized using Raman microspectroscopy.

Experimental part

In the experiment, a silicon wafer (thickness 380 nm, surface orientation 111) was ablated in a single-pulse mode. Air and distilled water were used as a buffer medium during ablation. The water layer above the sample surface was 2–3 mm

The scheme of the experiment is shown in Fig. 1, *a*. As a source of laser radiation, we used a Satsuma fiber laser (Amplitude Systems) with an active medium on Yb^{+3} ions (fundamental harmonic wavelength 1030 nm, pulse repetition rate 0–2 MHz). The study of craters was carried

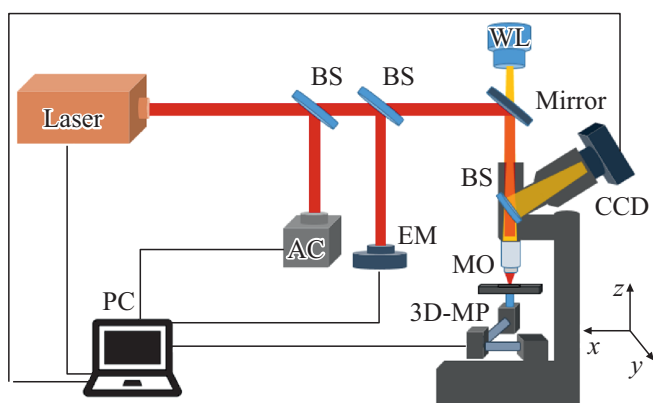


Figure 1. Experimental unit scheme. Satsuma laser, SHG — Second Harmonic Generator, BS — Beam Splitter, EM — Energy Meter, AC — Autocorrelator, MO — Numerical Aperture Microlens $N_A = 0.25$, WL — white light source, 3D-MP — three-axis motorized platform.

out for durations of 0.3 and 10 ps. The ULP energy in the TEM₀₀ mode was smoothly varied using a thin-film reflective attenuator. Laser radiation was focused onto the sample surface through an objective with a numerical aperture $N_A = 0.25$ and a focal length of 7.50 mm into a spot $3.2\ \mu\text{m}$ according to the intensity level of the Gaussian beam $1/e$.

Raman spectra were recorded on a U-1000 spectrometer by ISA Jobin-Yvon (France). The device is equipped with an optical microscope allowing to optically single out the studied surface of a sample up to $1 \times 1\ \mu\text{m}$ in size. An argon laser (514.53 nm) was used as a source of laser radiation. The output radiation power was not less than 50 mW. All sample measurements were performed in the „reflection“ geometry. For a lens with a numerical aperture of $N_A = 0.95$ and the wavelength used, the focusing size (spot diameter D) will be equal to [5]

$$D = \frac{0.61\lambda_0}{N_A}. \quad (2)$$

The penetration depth of laser radiation into silicon D_p can be calculated by the formula [17]

$$D_p = \frac{2.3}{2\alpha(\lambda_0)}, \quad (3)$$

where λ_0 — wavelength of exciting radiation, α — absorption coefficient for the given wavelength ($14.96\ \text{cm}^{-1}$). Values obtained: $D \approx 0.63\ \mu\text{m}$, $D_p \approx 0.77\ \mu\text{m}$.

Results and discussions

For craters on silicon, the RS spectra were studied in the region $400\text{--}560\ \text{cm}^{-1}$. Spectra were obtained for several regions of the craters. This is a side (edge), an area inside and outside the crater. When examining a crater with a thin transitional boundary a problem arose. When

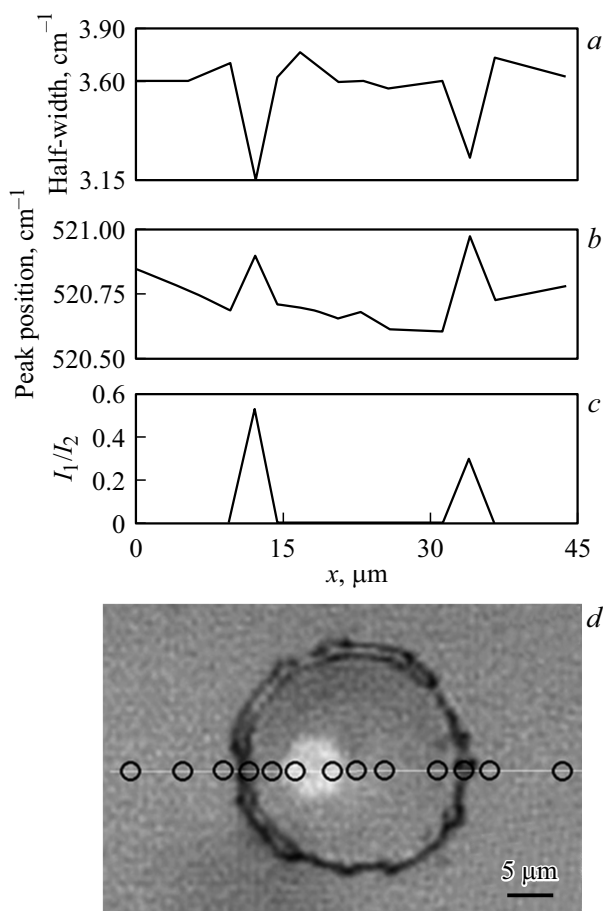


Figure 2. The change in the properties of the Raman peak of the fundamental vibration Si depending on the place of registration: *a* — dependence of the half-width; *b* — frequency dependence; *c* — manifestation of peak asymmetry, *d* — photograph of the sample, on which the registration points of the Raman spectra are marked.

sequentially scanning a sample, in order to be ensure, that the laser excitation spot reaches the boundary, the scanning step should be smaller, than the boundary thickness and the laser spot diameter (which are approximately equal). This will take too long. To solve this problem we used the following method. Manually the spot of laser excitation was aligned with the sample region of interest. After recording the RS spectrum, the sample image in the microscope field was recorded and stored. The process was repeated for all measurements. Further, the program created by us determined the shift of one image relative to another, and thus we obtained a sample map and points on it, where RS spectra were recorded. Figure 2, *d* shows an optical image of the crater, on which the points where the RS spectra were recorded are marked.

It can be seen from the plots for the half-width (Fig. 2, *a*) and frequency (Fig. 2, *b*), that the half-width of the peak practically does not change, and the position of the maximum decreases in frequency in the crater center. Note, that the shape of the peaks is always symmetrical, except

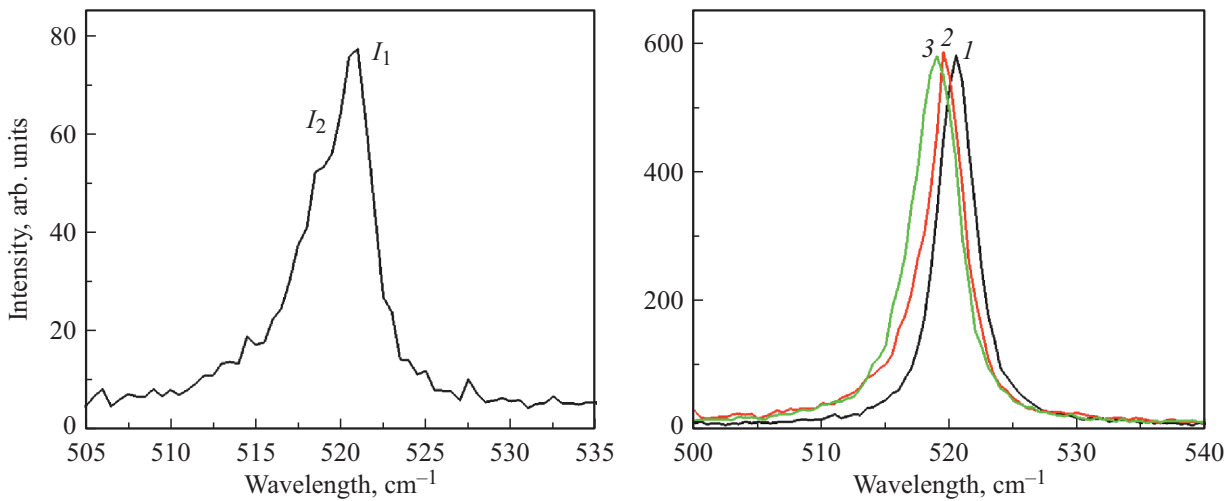


Figure 3. *a* — RS spectrum at the crater boundary; *b* — RS spectra from different points of the crater boundary (curves 2, 3) and the initial single crystal (*I*).

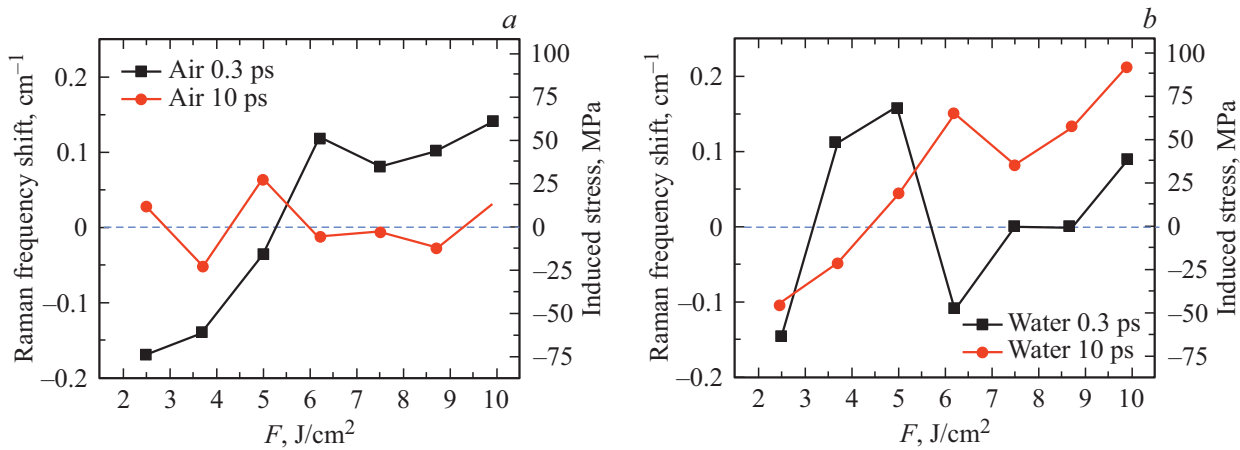


Figure 4. Main peak shifts relative to pure silicon from the energy for pulse durations of 0.3 and 10 ps during ablation: *a* — in air, *b* — in water.

for the boundary. This is due to the occurrence of local stress during laser machining.

Directly at the crater boundary (Fig. 2, *a, b*) we see a decrease in the half-width and an increase in the frequency of the silicon RS peak. This happens, as for RS peak in this area an asymmetry in the shape appears, and we make an approximation along the two arms of this peak (Fig. 3, *a*). For a qualitative demonstration of the asymmetry, we approximated the RS bands with two symmetrical bands and plotted the ratio of the intensities of these bands on the graph (Fig. 2, *c*). This is a purely qualitative approach. Therefore, the data for the graphs in Fig. 2, *a, b* at the points corresponding to the crater boundaries do not make much sense.

Let us consider in detail the Raman spectra directly at the crater boundary. As already mentioned, for this region we always observe an asymmetry in the shape of RS band of the silicon fundamental vibration (Fig. 3, *a*). It is also seen from this spectrum, that the band is a composite —

there is clearly a 521 cm⁻¹ single-crystal silicon band and an asymmetric band with a lower frequency.

This occurs, because the width of the crater boundary and the diameter of the exciting radiation spot are close, and both the crater boundary and single-crystal regions can be recorded simultaneously. For a more correct registration of the RS spectrum from the boundary, craters obtained at the highest energy density and having the largest rim thickness were selected. Figure 3, *b* shows examples of such spectra. We attribute the shift and the resulting asymmetry of the main peak to the formation of nanocrystals in this region. The size of nanocrystals can be calculated from the $\Delta\omega$ shift of the silicon phonon mode [18]:

$$\Delta\omega(D) = -A\left(\frac{\alpha}{D}\right)^\gamma, \tag{4}$$

where $\Delta\omega(D)$ — shift of the RS band in nanostructures D in diameter, α — lattice constant Si (0.543 nm), D —

nanostructure diameter, $\gamma = 1.44$ — approximation parameters describing phonon localization in nanometer spheres with the diameter D in diameter, A — empirical value (47.74 cm^{-1}). Using this formula and the obtained data on the shift of the RS bands gives an estimate of $D \sim 7\text{--}8 \text{ nm}$.

The shifts of the silicon RS bands in the center of craters were compared depending on the duration and energy (Fig. 4). The calculation of the emerging stresses was carried out according to the formula (1). The minimum effect was manifested at the minimum intensity of the laser pulse (10 ps in air), at which the voltages change weakly with energy and are within $13\text{--}22 \text{ MPa}$. At high energy densities (more than 5 J/cm^2), a shift of the RS peak to the long wavelength region is observed for ablation in air for 0.3 ps and in liquid 10 ps, which corresponds to the appearance of compressive stresses in the near-surface layer. The voltage values at the maximum energy density reach 91 MPa. At the same time, for these conditions, but at lower energy densities, the peak shifts to the short-wave region, which corresponds to tensile stresses, when recalculating the components -63 MPa .

For ablation in liquid (Fig. 4, b) with a pulse duration of 0.3 ps and energy densities above 5 J/cm^2 , we have noticed in the study [19], the appearance of filamentation at the critical laser radiation power $\approx 4\text{--}6 \text{ MW}$, which reduces the effective energy density reaching the target surface. We observe the display of this effect for the emerging stresses in silicon. At the maximum energy (9.9 J/cm^2) compressive stresses arise, which are two times less, than during ablation in air. The jump in the local voltage in the region 5 J/cm^2 can be associated with a transition to the subfilamentation regime, a further decrease in the energy density leads to a decrease in the resulting stresses, and then they become negative. This means, that the dependence in the subfilamentation mode behaves in the same way, as the dependences during ablation in air for 0.3 ps and in liquid for 10 ps.

During ablation in liquid for 10 ps ablation is performed in the subfilamentation mode, and the highest compressive stresses are observed due to the fact, that the water layer restrains the broadening of the region with ablation products, thereby increasing the shock wave amplitude [20].

Conclusion

In the present study the silicon surface was modified in the single-pulse mode by femto-picosecond laser pulses (0.3 10 ps) in the near-IR range (1030 nm) during ablation in air and in water. The resulting structures were studied using Raman microscopy. It has been found, that nanocrystallites of 7–8 nm size appear on the crater boundary. Local mechanical stresses, which arise in the crater center, the sign of which depends on the applied energy density, were found. The greatest local compressive stresses arise in water during the subfilamentation mode at maximum energy densities.

The minimum stresses arise during ablation in air under the action of laser radiation with a pulse duration of 10 ps.

Conflict of interest

The authors declare that they have no conflict of interest.

References

- [1] Chichkov B.N. et al. // Appl. Phys. A. 1996. V. 63. N 2. P. 109–115. doi 10.1007/BF01567637
- [2] Neuenschwander B. et al. // Phys. Proc. 2014. V. 56. P. 1047–1058. doi 10.1016/j.phpro.2014.08.017
- [3] Smirnov N.A. et al. // JETP Letters. 2018. V. 108. N 6. P. 368–373. doi 10.1134/S002136401818011X
- [4] Smirnov N.A. et al. // Opt. and Quant. Electron. 2020. V. 52. N 2. P. 1–8. doi 10.1007/s11082-019-2169-1
- [5] Sheremet E. et al. // Phys. Stat. Sol. (a). 2019. V. 216. N 19. P. 1900106.
- [6] Amer M.S., El-Ashry M.A., Dosser L.R., Hix K.E., Maguire J.F., Irwin Bryan. // Appl. Surface Sci. 2005. V. 242. N 1–2. P. 162–167. doi 10.1016/j.apsusc.2004.08.029
- [7] Ma L., Qiu W., Fan X. // Microelectronics Reliability. 2021. V. 118. P. 114045. doi 10.1016/j.microrel.2021.114045
- [8] Wolf I.D. // J. Raman Spectrosc. 1999. V. 30. N 10. P. 877–883. doi 10.1002/(SICI)1097-4555(199910)30:10<877::AID-JRS464>3.0.CO;2-5
- [9] Kang Y. et al. // Optics and Lasers in Engineering. 2005. V. 43. N 8. P. 847–855. doi 10.1016/j.optlaseng.2004.09.005
- [10] Xing Ma L. et al. // AIP Advances. 2019. V. 9. N 1. P. 015010.
- [11] Campbell I.H., Fauchet P.M. // Solid State Commun. 1986. V. 58. N 10. P. 739–741. doi 10.1016/0038-1098(86)90513-2
- [12] Richter H., Wang Z.P., Ley L. // Solid State Commun. 1981. V. 39. N 5. P. 625–629. doi 10.1016/0038-1098(81)90337-9
- [13] Periasamy S. et al. // Zeitschrift für Physikalische Chemie. 2017. V. 231. N 9. P. 1585–1598. doi 10.1515/zpch-2016-0961
- [14] Viera G., Huet S., Boufendi L. // J. Appl. Phys. 2001. V. 90. N 8. P. 4175–4183. doi 10.1063/1.1398601
- [15] Bonse J., Brzezinka K.W., Meixner A.J. // Appl. Surface Sci. 2004. V. 221. N 1–4. P. 215–230. doi 10.1016/S0169-4332(03)00881-X
- [16] Kiani A., Venkatakrishnan K., Tan B. // Optics Express. 2009. V. 17. N 19. P. 16518–16526. doi 10.1364/OE.17.016518
- [17] De Wolf I. // Semiconductor Science and Technology. 1996. V. 11. N 2. P. 139.
- [18] Periasamy S. et al. // Zeitschrift für Physikalische Chemie. 2017. V. 231. N 9. P. 1585–1598. doi 10.1515/zpch-2016-0961
- [19] Smirnov N.A. et al. // Appl. Surface Sci. 2021. V. 562. P. 150243. doi 10.1016/j.apsusc.2021.150243
- [20] Anisimov S.I. et al. // J. Physics: Conference Series. IOP Publishing. 2020. V. 1556. N 1. P. 012004. doi 10.1088/1742-6596/1556/1/012004